Atmos. Meas. Tech., 8, 3209–3218, 2015
www.atmos-meas-tech.net/8/3209/2015/
doi:10.5194/amt-8-3209-2015

Atmospheric Measurement Techniques
Open Access

Schneefernerhaus as a mountain research station for clouds and turbulence

S. Risius[1], H. Xu[1], F. Di Lorenzo[1], H. Xi[1], H. Siebert[2], R. A. Shaw[3], and E. Bodenschatz[1,4,5]

[1]Max Planck Institute for Dynamics & Self-Organization (MPIDS), 37077 Göttingen, Germany
[2]Leibniz Institute for Tropospheric Research, 04318 Leipzig, Germany
[3]Department of Physics, Michigan Technological University, Houghton, MI 49931, USA
[4]Institute for Nonlinear Dynamics, University of Göttingen, 37077 Göttingen, Germany
[5]Laboratory of Atomic and Solid State Physics and Sibley School of Mechanical and Aerospace Engineering, Cornell University, Ithaca, NY 14853, USA

Correspondence to: H. Xu (haitao.xu@ds.mpg.de) and E. Bodenschatz (eberhard.bodenschatz@ds.mpg.de)

Received: 16 December 2014 – Published in Atmos. Meas. Tech. Discuss.: 15 January 2015
Revised: 11 June 2015 – Accepted: 23 June – Published: 13 August 2015

Abstract. Cloud measurements are usually carried out with airborne campaigns, which are expensive and are limited by temporal duration and weather conditions. Ground-based measurements at high-altitude research stations therefore play a complementary role in cloud study. Using the meteorological data (wind speed, direction, temperature, humidity, visibility, etc.) collected by the German Weather Service (DWD) from 2000 to 2012 and turbulence measurements recorded by multiple ultrasonic sensors (sampled at 10 Hz) in 2010, we show that the Umweltforschungsstation Schneefernerhaus (UFS) located just below the peak of Zugspitze in the German Alps, at a height of 2650 m, is a well-suited station for cloud–turbulence research. The wind at UFS is dominantly in the east–west direction and nearly horizontal. During the summertime (July and August) the UFS is immersed in warm clouds about 25 % of the time. The clouds are either from convection originating in the valley in the east, or associated with synoptic-scale weather systems typically advected from the west. Air turbulence, as measured from the second- and third-order velocity structure functions that exhibit well-developed inertial ranges, possesses Taylor microscale Reynolds numbers up to 10^4, with the most probable value at ~ 3000. In spite of the complex topography, the turbulence appears to be nearly as isotropic as many laboratory flows when evaluated on the "Lumley triangle".

1 Introduction

Clouds play a crucial role in the thermal balance and the hydrologic cycle of the earth. Our understanding of the formation and evolution of clouds, however, is far from making reliable predictions. The difficulty is partially rooted in the turbulent nature of clouds due to the wide range of scales involved in the process (Jonas, 1996). In recent years, there has been increasing awareness of the importance of turbulence on clouds (Shaw, 2003; Bodenschatz et al., 2010; Devenish et al., 2012). The study of cloud–turbulence interaction is difficult since both laboratory experiments and numerical simulations cannot reproduce all the important physical and thermodynamical parameters involved in real-world clouds. Observations in natural clouds are therefore an irreplaceable aspect of the investigation. Most of these observations are carried out with airborne campaigns that are limited in resolution by the flying speed of the aircraft, even though significant progress has been achieved in recent years by using slowly flying instruments to improve spatial resolution (Siebert et al., 2006, 2010; Malinowski et al., 2013). Ground-based measurements at high-altitude research stations therefore play a complementary role. In this work, we consider the Umweltforschungsstation Schneefernerhaus (UFS) located just below the peak of Zugspitze in the German Alps, at a height of 2650 m. Several short campaigns on cloud research used UFS/Zugspitze as the measurement site (Siebert and Teichmann, 2000; Wirth et al., 2012). Here, by using the meteorological data (wind speed, direction, tem-

perature, humidity, visibility, etc.) collected by the German Weather Service (DWD) from 2000 to 2012 and turbulence measurements recorded by multiple ultrasonic sensors (sampled at 10 Hz) in 2010, we show that UFS is a well-suited station for cloud–turbulence research. Note that our work is not concerned with the climatology or mountain meteorology at Zugspitze, which are important problems by themselves and require different methods of study, e.g., using data from longer periods. Rather, by analyzing data recorded at UFS in the same way as conventionally done for laboratory flows, we show that both the turbulence and the cloud properties at UFS carry similar characteristics to those in other well-studied turbulent flows and in airborne clouds. Our results presented here can also serve as a benchmark characterization of the turbulence and cloud physics conditions at UFS, which can be used for other researchers who are interested in carrying out related studies at UFS to evaluate the usefulness of the research station for their own investigation.

In this paper, we present the flow conditions and large-scale turbulence at UFS. The small-scale turbulence will be characterized in an accompanying paper (Siebert et al., 2015). Here, the term "large scale" or "forcing scale" corresponds to the range of the local peak in the energy spectrum and is related to the scale at which the kinetic energy is supplied into the turbulent motion; "small scale" or "dissipation scale" refers to the range at which the viscous dissipation converts the kinetic energy into heat. In-between lies the "inertial (sub)range", which is the range of scales where the kinetic energy is cascaded down to smaller and smaller scales without significant loss. This nomenclature is conventional in the fluid mechanics community (see, e.g., the following textbooks: Monin and Yaglom, 1971, 1975; Tennekes and Lumley, 1972; Frisch, 1995; Pope, 2000) and is also widely adopted in other related communities, e.g., in astrophysics (Mac Low and Klessen, 2004) and in atmospheric science (Wyngaard, 2010). In meteorology sometimes the entire range of scales where turbulence dynamics are important is defined simply as "microscale turbulence", in contrast with the "macroscale turbulence" of the large-scale synoptic flows (Etling, 2008). We will discuss in more detail these different terminologies later in relation to the energy spectrum measured at UFS.

2 Geography and environment

UFS (47°25′00″ N, 10°58′46″ E) is located near the top of Zugspitze, which is the highest mountain in Germany, at a height of 2962 m above sea level. UFS is a nine-story building, constructed into the southern flank of the Zugspitze (see Fig. 1). The southern flank of the mountain is covered with Germany's largest glacier, the Schneeferner, which is surrounded by a mountain arc that shields it from winds coming from the north, west and south. The Schneeferner is unshielded towards the south-east where melt water streams

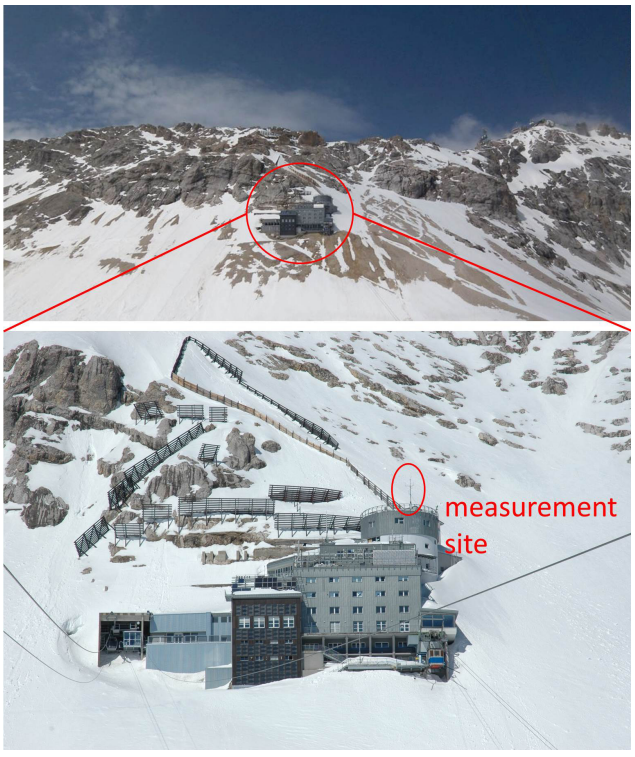

Figure 1. Views of UFS from the south. The lower picture is a close-up view of the top picture, and the measurement site is indicated by the red ellipse. The photo shown in the top panel was taken in May 2007 and that in the bottom panel was taken in October 2009.

run down the mountain. UFS is situated on the north side of the glacier, at a height of about 2650 m (see Fig. 2). The mountain ridge on the west of the glacier is known as the Schneefernerkopf. Over a length of about 200 m, erosion has decreased the height of the ridge significantly, and the lowest point is about 175 m lower than the Schneefernkopf summit (Engelbrecht, 2011). This part is known as the "wind hole", because it directs the wind from the west over the glacier, also over UFS, like a funnel.

The weather at Zugspitze is mainly influenced by the westerlies and synoptic-scale systems that lead to heavy precipitation on the northwest side of the Zugspitze massif. In addition to this, on about 60 days per year the weather is dominated by foehn winds, which push against the massif from the south, resulting in relatively high temperatures during the winter times. The average temperature at the peak of Zugspitze during the standard reference period (1961–1990) was −4.8 °C, while the lowest and the highest were −35.6 and 17.9 °C, respectively (DWD, 2000), and the average precipitation was 2003 mm per year (Siebler, 2010).

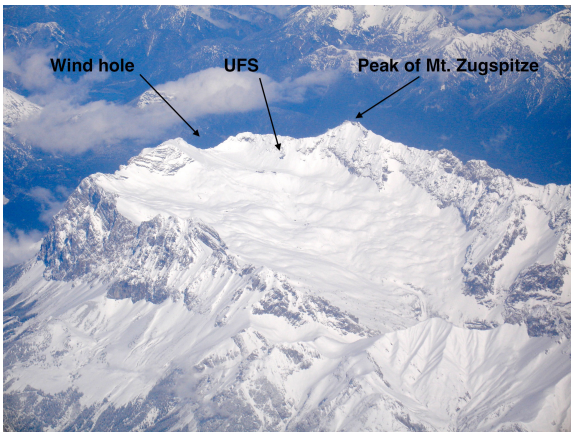

Figure 2. View of the Schneeferner valley from the south-east (Photo taken by Xtream, alpinforum.com Luftbilder Topic, 24 April 2009. http://www.alpinforum.com/forum/viewtopic.php?f=7&t=19048&start=50)

3 Flow conditions at UFS

Figure 3 shows the local weather conditions at UFS, including temperature, relative humidity, solar radiation and visibility, using the hourly data from the Deutscher Wetterdienst (DWD, German Weather Service) recorded between 2000 and 2012. The average temperature at UFS during that period, −1.5 °C, was higher than the average temperature at the peak of Zugspitze during the standard reference period. The hourly average temperature at UFS varies between −10 and +6 °C throughout the year. The average relative humidity is also nearly the same throughout the year, but with much larger fluctuations in wintertime. As a check, we analyzed the 1 min data between 2008 and 2012, also recorded by DWD. The results are the same as those from the hourly data over the same period. In the presentation below, the term "DWD data" refers to the recording over the longer period, i.e., the hourly data between 2000 and 2012.

We now turn to the flow and turbulence conditions at UFS, which is the main focus of this paper. To see the possible relation between clouds and the flow conditions, we define the "cloud" events as when the relative humidity is above 99 %. We varied this condition to when the relative humidity is above 95 %, and to include other conditions such as requiring the temperature to be above 0 °C or the visibility to be below 200 m. The statistics obtained are virtually the same. Figure 4 shows the probability density functions (PDFs) of the horizontal wind direction and the wind speed under both the no-clouds and clouds conditions. Note that we use the word "wind" to merely refer to air flow. Due to the local topography, the winds at UFS are primarily in the east–west direction. This dominance of a preferred wind direction is very convenient for fixed instruments, such as a hot-wire and particle size analyzer (see also the accompanying paper, Siebert et al., 2015). The variations of the wind direction and the PDF of wind speed are different for wind from the west and from the east, which is most likely due to the different topography on the two sides. Winds from the west have to pass over the mountain ridge before reaching UFS and hence are generally more intense and spread over wider angles. The east winds usually flow along the valley and are mostly free from the effect of the mountain. In comparison, the flow conditions (wind direction and wind speed) are almost independent of whether the wind is carrying clouds or not.

As a way to quantify the difference between the wind from the east and from the west, we fitted the wind speed PDFs shown in Fig. 4 as Weibull distributions. The shape parameters of the fitted Weibull distribution are 1.50, 1.48, 1.33 and 1.33 for wind from the east with clouds, wind from the east without clouds, wind from the west with clouds and wind from the west without clouds, respectively. As expected the shape parameter depends only on whether the wind is from the east or from the west, and it is not sensitive to whether there are clouds or not. In all cases the shape parameter of the fitted Weibull distribution is smaller than 2, which signals a wide distribution of wind speed. The shape parameter for wind from the east is slightly larger, which is consistent with the local topology; i.e., wind from the east is coming from the valley, with less influence by the mountain, while wind from the west is coming over the ridge, from the wind hole and moves along the mountain before reaching the measurement site.

As we are interested in the events of clouds covering UFS, we checked the time fraction of cloud covering at a given month of the year. Figure 5 shows that it is more likely to observe clouds in the "summer" (from April to September) than in the "winter" (from October to March). This is especially true for clouds from the east because these clouds are almost exclusively formed from the convection rising from the valley, which correlates with solar radiation. Clouds from the west can be carried by the dominating westerlies, as stated in Sect. 2, and therefore do not show a simple dependence on the season. On the other hand, there is still a pronounced peak around July. Overall, the probability that the UFS is covered in clouds is more than 25 % in the summer, with a peak of nearly 30 % in July. In the summer, the probability of having clouds from the east and the west is approximately 10 and 15 %, respectively. Therefore, the UFS offers a good possibility to compare these two types of clouds and the associated turbulence.

To evaluate the chance of measuring clouds, we also checked the cloud fraction during the time of the day in summer and in winter, as shown in Fig. 6. In the summertime the clouds are most likely to occur during the late afternoon and later in the night, which reflects the fact that the summer clouds are usually formed from convection originated in the local valley. During the wintertime the probability of cloud occurrence is independent of the time of day, suggesting that cloud cover is more associated with synoptic-scale weather.

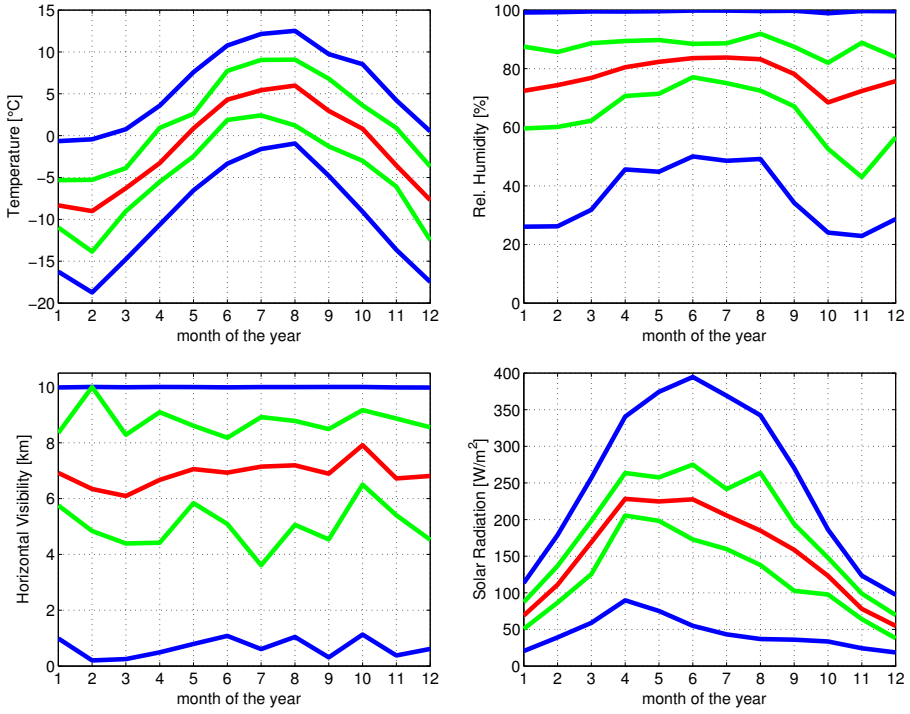

Figure 3. Local weather conditions at UFS, obtained from recordings by the Deutscher Wetterdienst (DWD, German Weather Service) over the years 2000–2012. More meteorological data recorded by DWD can be obtained from the ftp site: ftp://ftp-cdc.dwd.de/pub/CDC/. Red curves are the averages over that period; green curves are the minimum and maximum values of the monthly averages; and blue curves are the minimum and maximum values of the hourly averages.

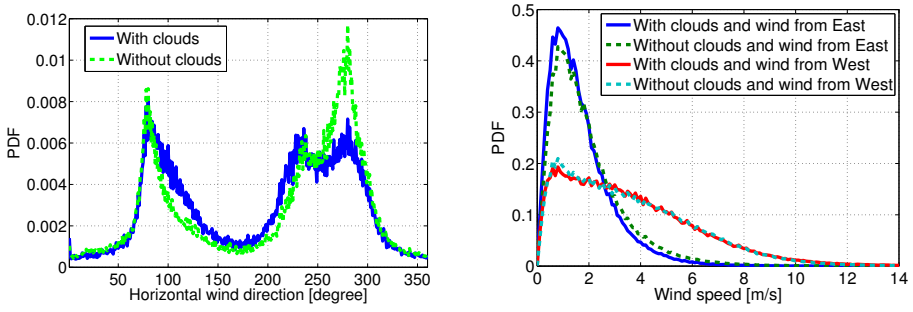

Figure 4. PDFs of the horizontal wind direction (left panel) and the wind speed (right panel). In the plot of the horizontal wind direction, 0° corresponds to the wind coming from the north, and 90 and 270° correspond to the wind from the east and the west, respectively. The condition for "clouds" is that the relative humidity be above 99 %.

4 Large-scale turbulence

To measure large-scale turbulence, we installed five ultrasonic sensors on a mast located on the roof of the round tower of the UFS (Fig. 1). The ultrasonic sensors are manufactured by Thies Clima (Göttingen, Germany), and each of them measures the full wind velocity vector in three dimensions at a sampling frequency of 10 Hz. The five sensors are arranged in a configuration that forms two tetrahedrons sharing one face (Fig. 7). The analysis shown here is mainly from the measurements by the top sensor, which is approximately 6 m above the roof and 20 m away from the mountain. The wind measured by this sensor is least influenced by the mast itself and other sensors. Figure 8 shows the spectrum of the horizontal wind velocity in the east–west direction (solid line), measured from the 1 min DWD data between January 2008 and July 2012 (circles), with our sonic sensor at 10 Hz between September 2010 and September 2011 (crosses). The sonic sensor spectrum shown was obtained by averaging the spectra from records of every 2 h and hence only extends between 0.5 h^{-1} and 5 Hz. The two spectra agree very well in the frequency range covered by both

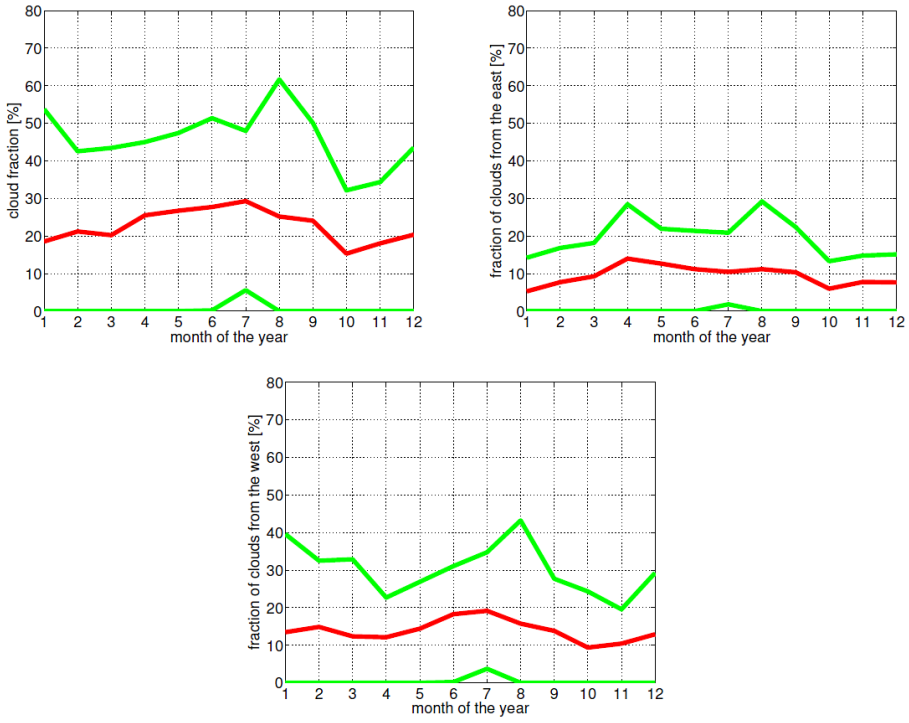

Figure 5. Fraction of time during which the UFS is covered by clouds during any month of the year. The red curve is the average cloud fraction, and the green curves are the maximum and minimum monthly values over the period of data analyzed. From the top to the bottom, the three panels are the total fraction of cloud covering, the fraction of clouds from the east and the fraction of clouds from the west.

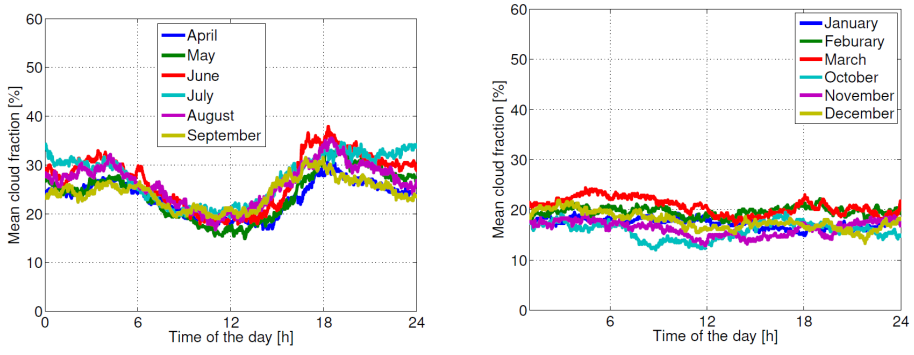

Figure 6. Average fraction of time that clouds cover UFS at a given time of the day (local time at UFS) in summer (top) and in winter (bottom).

data records, i.e., between $0.5\,\mathrm{h}^{-1}$ and $0.5\,\mathrm{min}^{-1}$. The peak at $f = 1.15 \times 10^{-5}$ Hz in the spectrum corresponds to the diurnal forcing. There is a noticeable "knee" at a frequency range of about $1\,\mathrm{h}^{-1}$, which can be made clearly visible from the compensated spectrum $f \cdot E(f)$ shown in the bottom panel of Fig. 8. This is the so-called "spectral gap" and is known to exist in spectra measured in many atmospheric flows, under vastly different geographic conditions (Stull, 1988). The spectral gap is commonly considered as the separation between the timescales of the synoptic flow and the local "microscale turbulence" that bears more universal features as assumed by the Kolmorogov hypotheses (Kolmogorov, 1941). In detailed turbulence studies such as we are concerned with here, it is customary to divide this range into large scales, small scales and the "inertial range" in between. The large scales are where the energy is supplied into the turbulent motion, which may be loosely related to the peak after the spectral gap in the compensated spectrum, i.e., at timescales of roughly 1 to 10 min. The small scales are at much faster timescales or much smaller length scales that are dominated by viscous dissipation, which cannot be resolved from the sonic sensor measurements.

To access the turbulence properties at faster timescales, we added the spectrum from a hot-wire anemometer mea-

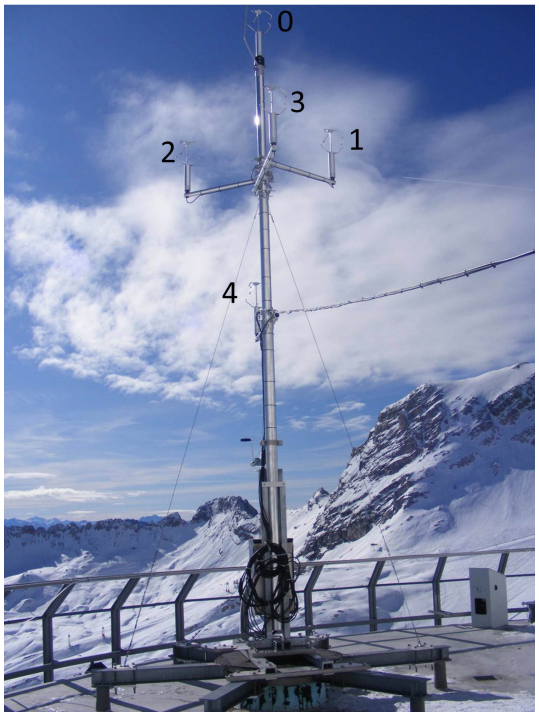

Figure 7. The ultrasonic wind sensors installed on the roof of UFS. The five ultrasonic sensors are labeled with numbers from 0 to 4. The top sensor (number 0) is approximately 6 m above the roof.

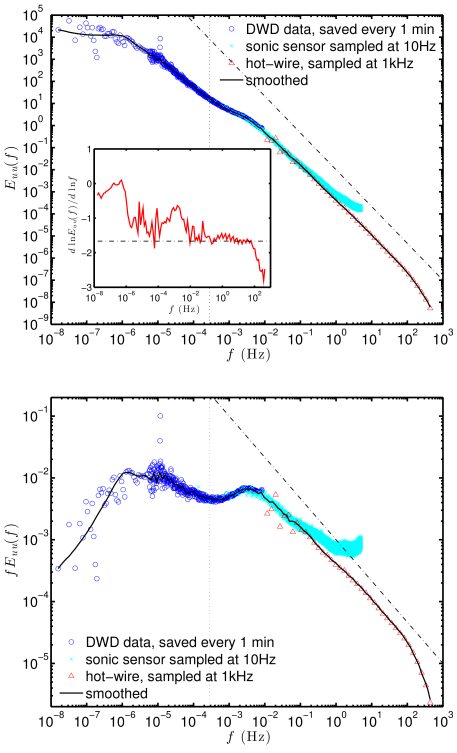

Figure 8. The composite spectrum of the east–west horizontal wind velocity, including data from the 1 min DWD recording between January 2008 and July 2012 (circles), measured from our sonic sensor sampling at 10 Hz between September 2010 and September 2011 (crosses), and from a one-component hot-wire anemometry sampled at 1 kHz in August 2009 (triangles). The thick solid line is a smoothed composite spectrum using all three spectra mentioned above. Note that, due to the limited resolution, the 10 Hz sonic sensor data deviate from the hot-wire data at $f \gtrsim 10^0$ Hz and are not used beyond that. The Kolmogorov $E_{\mathrm{uu}}(f) \propto f^{-5/3}$ spectrum was shown for comparison (dash-dotted line). Note that it gives $f E_{\mathrm{uu}}(f) \propto f^{-2/3}$ in the compensated plot in the bottom panel. The vertical dotted line marks the frequency corresponding to a 1 h period. The inset of the top panel shows the local slope $\mathrm{d}\ln E/\mathrm{d}\ln f$ of the smoothed spectrum, from which the scaling range can be identified. The bottom panel shows the compensated spectrum $f \cdot E_{\mathrm{uu}}(f)$, in which the so-called "spectral gap" at $f \approx 1\,\mathrm{h}^{-1}$ is clearly visible.

surement sampled at 1 kHz, which was conducted in August 2009 (triangles). The hot-wire spectrum overlaps well with the spectrum from the sonic sensor in the range of frequency between 10^{-2} and 10^{-1} Hz. The deviation of the sonic sensor spectrum is most likely due to its limited resolution in wind velocity measurement. The composited spectrum from all three spectra shows that, for flows at UFS, the spectrum at $10^{-2} \lessapprox f \lessapprox 10^{2}$ Hz indeed follows the Kolmogorov spectrum $E_{\mathrm{uu}}(f) \propto f^{-5/3}$, which is shown by the dash-dotted lines in both panels of Fig. 8. Note that it gives $f E_{\mathrm{uu}}(f) \propto f^{-2/3}$ in the compensated plot. As suggested by Fig. 8, in our following analysis of the turbulence, we divide our records to segments that are no longer than 10 min.

We now study quantitatively the turbulent flows at UFS. We present here large-scale flow measurements. Analysis of small-scale turbulence is reported in an accompanying paper (Siebert et al., 2015). We analyzed in detail the continuous recording of wind velocities by the top sensor between September and December 2010. From these recordings, we select the "steady" events that are defined as segments with periods between 1 and 2 min, during which the fluctuation of wind around its mean is less than 25 % of the mean. For these segments, we then used Taylor's frozen turbulence hypothesis to obtain spatial correlations and structure functions from the time series of velocity data. The longitudinal and transverse velocity auto-correlations, $f(r,t)$ and $g(r,t)$, are defined as

$$f(r,t) = \frac{\langle u_1(\boldsymbol{x}+\boldsymbol{e}_1 r,t)u_1(\boldsymbol{x},t)\rangle}{\langle u_1^2\rangle}, \quad (1)$$

$$g(r,t) = \frac{\langle u_{2,3}(\boldsymbol{x}+\boldsymbol{e}_1 r,t)u_{2,3}(\boldsymbol{x},t)\rangle}{\langle u_{2,3}^2\rangle}, \quad (2)$$

where the subscripts 1, 2 and 3 refer to vector components and $\boldsymbol{e}_1$ is an unit vector in the 1 direction. Component 1 is the mean flow direction of the segment, which could vary from segment to segment, e.g., from east to west, and the other two components are in the directions perpendicular to the mean

velocity. The longitudinal and transverse integral scales, L_{LL} and L_{NN}, are

$$L_{\mathrm{LL}}(t) = L_{11}(t) \equiv \int_0^\infty f(r,t)\mathrm{d}r, \tag{3}$$

$$L_{\mathrm{NN}}(t) = L_{22,33}(t) \equiv \int_0^\infty g(r,t)\mathrm{d}r. \tag{4}$$

Since an integration up to infinity is practically not possible, we determine the integral length scales by integrating correlations up to the first zero-crossing. The integral length scales correspond roughly to the sizes of the biggest eddies in the flow and therefore vary significantly in environmental flows. Figure 9 show the distribution of the measured integral length scales. The most probable values of the longitudinal and transverse length scales are $L_{\mathrm{LL}} \approx 9\,\mathrm{m}$ and $L_{\mathrm{NN}} = (L_{22}+L_{33})/2 \approx 4.5\,\mathrm{m}$, which agree surprisingly well with the relation of $L_{\mathrm{LL}} = 2L_{\mathrm{NN}}$ for homogeneous and isotropic turbulence (e.g., Pope, 2000). We note that these values are also consistent with the measurement height of 6 m and are not necessarily representative of the largest eddies in the atmospheric boundary layer, which could possess much bigger scales (Wyngaard, 2010).

On the other hand, the averages of the instantaneous length scale ratio is $\left\langle \frac{L_{\mathrm{LL}}}{L_{\mathrm{NN}}} \right\rangle = 1.51$, which indicates that the large-scale wind conditions at the measurement site are in fact anisotropic. This large-scale anisotropy may be explained by wind shear induced by surrounding structures. A 6 m tall lidar tower located in the northwest of the measurement site blocks the flow from that direction. Because of the presence of the lidar tower, wind coming from the west experiences a strong shear at the measurement site. In contrast, wind coming from the east is less influenced because no structures are located on the east side of the measurement site. Indeed, the average length scale ratio $\left\langle \frac{L_{\mathrm{LL}}}{L_{\mathrm{NN}}} \right\rangle$ is 1.79 for east winds and 1.26 for west winds, which also suggests that the east wind is in general more isotropic.

Energy dissipation rate per unit mass, ε, is the most important quantity to characterize turbulence. For cloud studies, the turbulence energy dissipation rate determines the other parameters of cloud droplets such as the Stokes number and the settling parameter (Siebert et al., 2010). We estimate the energy dissipation rate from the longitudinal and transverse second-order velocity structure functions by fitting the inertial range scaling:

$$D_{\mathrm{LL}} = C_2(\varepsilon r)^{2/3} \tag{5}$$

and

$$D_{\mathrm{NN}} = \frac{4}{3}C_2(\varepsilon r)^{2/3} \tag{6}$$

with a value of $C_2 = 2.1$ (e.g., Pope, 2000). As shown in the top panel of Fig. 10, the measured structure functions

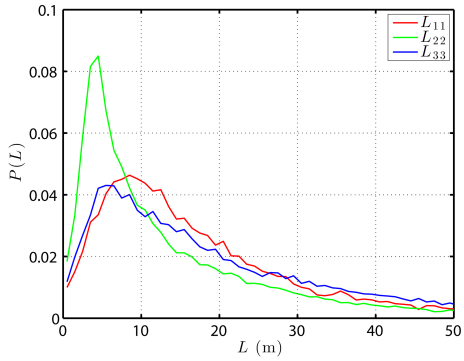

Figure 9. PDFs of the integral length scales measured using Taylor's hypothesis. Note that L_{11} corresponds to the longitudinal integral scale L_{LL} and L_{22} and L_{33} correspond to the transverse integral scale L_{NN}. The most probable value of L_{LL} is 9 m, and the most probable values of the transverse scales are $L_{22} \approx 4\,\mathrm{m}$ and $L_{33} \approx 5\,\mathrm{m}$.

D_{LL} and D_{NN} indeed show a scaling region consistent with Eqs. (5) and (6), where we fit for ε. We then check these values against the measured third-order structure function, which satisfies an exact scaling law

$$D_{\mathrm{LLL}} = -\frac{4}{5}\varepsilon r. \tag{7}$$

As shown in the bottom panel of Fig. 10, the measured values of D_{LLL} are within a factor of 2 from the lines $-\frac{4}{5}\varepsilon r$ with the energy dissipation rates ε estimated from the second-order velocity structure functions D_{LL} and D_{NN}. It is known that the scaling of the third-order structure function, Eq. (7), is more sensitive to Reynolds number, noise and the inhomogeneity of the flow (Xu et al., 2009; Mydlarski and Warhaft, 1996). We therefore take the averages of the values obtained using Eqs. (5) and (6) as the measured ε. The energy dissipation rates determined in this way are in the range of 10^{-4} to $10^{-2}\,\mathrm{m^2\,s^{-3}}$, which are comparable with previously reported values of atmospheric turbulence measurements (Wyngaard, 2010) and are also typical for turbulence in clouds (Siebert et al., 2006).

Using the measured values of ε and the rms velocity fluctuation u, we estimate the Taylor microscale Reynolds number for each segment as

$$R_\lambda = \sqrt{15\frac{u^4}{\varepsilon\nu}}, \tag{8}$$

where ν is the kinematic viscosity of air. This definition assumes that the turbulence is homogeneous and isotropic (e.g., Pope, 2000) and that the largest length scale can be estimated as $L \sim u^3/\varepsilon$, which we discuss next. The PDF of R_λ obtained using Eq. (8) is shown in Fig. 11. The maximum Reynolds number measured is $R_\lambda \sim O(10^4)$, and the most probable value is $R_\lambda \approx 3000$.

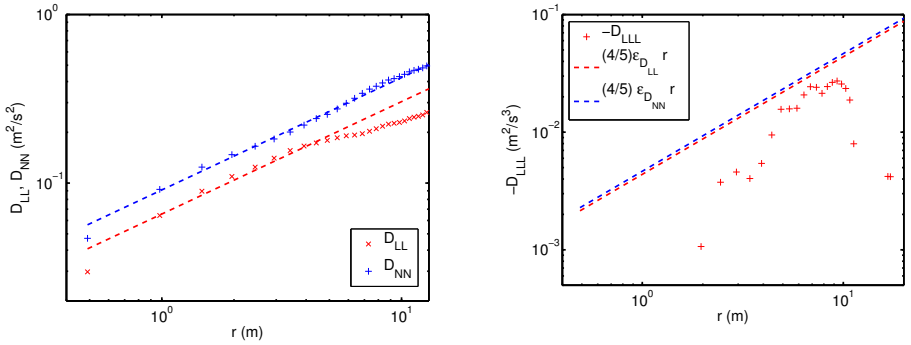

Figure 10. The second-order (top panel) and the third-order (bottom panel) velocity structure functions obtained from the ultrasonic sensor data. The dashed lines in the top panel are fits to Eqs. (5) and (6), which give the values of ε. These values are then used in Eq. (7) to plot the two dashed lines in the bottom panel.

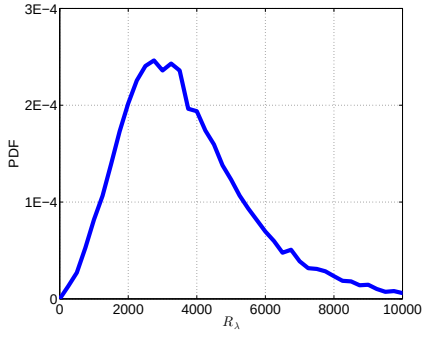

Figure 11. PDFs of the Taylor-scale Reynolds number R_λ. The most probable value is $R_\lambda \approx 3000$.

With the values of ε, L and u, we check the normalized energy dissipation rate

$$C_\varepsilon = \frac{\varepsilon L}{u^3}. \tag{9}$$

It has been found that the normalized energy dissipation rate C_ε is a constant of approximately 0.5 for a wide range of Reynolds numbers, including both laboratory flows and flows in the atmosphere (Burattini et al., 2005; Pearson et al., 2002; Sreenivasan, 1998). This observation has also been called the "zeroth law of turbulence", as Kolmogorov's hypotheses assume that the mean energy dissipation rate is independent of the viscosity at high Reynolds numbers (Frisch, 1995; Pearson et al., 2004).

Figure 12 shows the current measurements of C_ε as a function of Reynolds number. In agreement with earlier measurements, a value of about 0.5 was found. It can also be seen that the value of C_ε depends weakly on the wind direction, which may be attributed to the different flow conditions of the east and the west wind. As described before, winds from the west are subject to stronger shear than winds from the east. Previous data from turbulence in homogeneous shear flows showed that, in shear flows, ε estimated from isotropic relations is smaller than the true energy dissipation

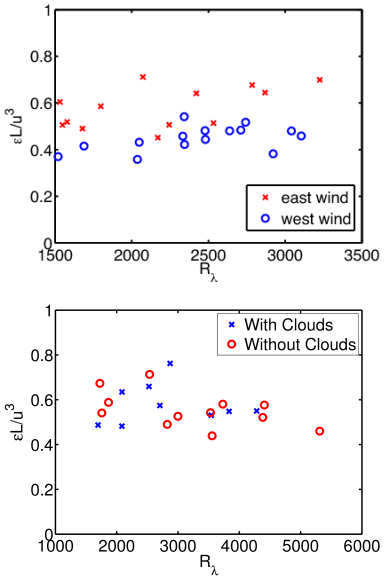

Figure 12. Normalized energy dissipation rates conditioned on wind direction (top) and cloudiness (bottom).

rates (Sreenivasan, 1995). Therefore, for wind from the west, the measured C_ε could be smaller than the real values. On the other hand, the effect of clouds on the normalized energy dissipation rate C_ε is not very clear. There might be a slight increase in C_ε associated with the occurrence of clouds, but better converged data are needed before drawing any conclusions.

Finally, to further investigate the deviation of the turbulent flow at UFS from the ideal isotropic conditions, we show the measured events on the so-called "Lumley triangle", which is the realizable region on the plane spanned by the two non-trivial invariants of the deviatoric part of the Reynolds stress tensor (Schumann, 1977; Lumley and Newman, 1977; Pope, 2000). The top curved side of the "triangle" represents two-component turbulence; i.e., one component of the fluctuating

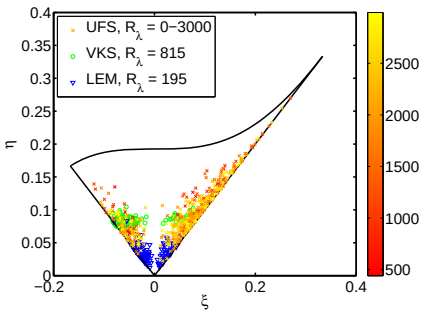

Figure 13. Mapping of the eastward turbulent wind flows at UFS on the Lumley triangle, in comparison with two laboratory flows: the von Kármán flow and the LEM flow. Here η and ξ are the two non-trivial invariants of the Reynolds stress tensor (Schumann, 1977; Lumley and Newman, 1977; Pope, 2000). The symbols representing the UFS flows are color-coded with the Reynolds number R_λ, whose range is indicated by the colorbar.

velocity vanishes, e.g., $\langle u_1^2 \rangle = 0$, or is much smaller than the other two components. Both of the two straight sides of the triangle represent axisymmetric turbulence, i.e., two components of the fluctuations are the same, e.g., $\langle u_2^2 \rangle = \langle u_3^2 \rangle$. The left side corresponds to the state of the third component being smaller than the other two, e.g., $\langle u_2^2 \rangle = \langle u_3^2 \rangle > \langle u_1^2 \rangle$, which may be termed as "axisymmetric turbulence with one smaller eigenvalue" (Pope, 2000); while the right side corresponds to the opposite state: i.e., the third component is larger than the other two, e.g., $\langle u_1^2 \rangle > \langle u_2^2 \rangle = \langle u_3^2 \rangle$, which can be similarly termed as "axisymmetric turbulence with one larger eigenvalue" (Pope, 2000). When mapped onto that plane, any realistic turbulent flow must lie within the Lumley triangle. The origin on that map represents the isotropic flows. The closer to the origin, the more isotropic the flow is. As shown in Fig. 13, the flows at UFS (for winds from the east) are not strictly isotropic. In fact, the turbulence is close to being axisymmetric, with both "one smaller eigenvalue" and "one larger eigenvalue" cases. As the Reynolds number increases, however, there is a trend for the flow to become more isotropic. We also compared the flows at UFS with two widely used laboratory turbulent flows, i.e, the von Kármán swirling flow between two counter-rotating disks (La Porta et al., 2001; Mordant et al., 2001; Bourgoin et al., 2006) and the propeller-driven turbulent flow within an icosahedra, named the Lagrangian exploration module, or LEM (Zimmermann et al., 2010). The turbulent flows at UFS are less isotropic than the LEM flow, which is designed to achieve high homogeneity and isotropy (Zimmermann et al., 2010). On the other hand, the degree of isotropy of the UFS flows is comparable and, in many cases, even better than the von Kármán flow, especially as the Reynolds number increases. For winds from the west, the range of anisotropy is approximately the same as that of the east winds, but no clear change with Reynolds number can be observed. This is most likely due to the effect of shear as discussed before.

5 Conclusions

From our analyses of both meteorological data and the turbulent flow data, we can conclude that the research station UFS is suited for cloud–turbulence interaction studies. The turbulence characteristics at large scales are similar to other laboratory flows, especially for winds coming from the east, which are less influenced by the building structures and nearby mountain. In addition to the analyses of small-scale turbulence, we are also analyzing the spatial structures of the turbulence using the multi-point correlations obtained from simultaneous measurements of the five ultrasonic sensors. The results will be reported elsewhere.

Acknowledgements. We thank Szymon Malinowski, Alain Pumir, and Jörg Schumacher for helpful discussions during this work. We are grateful to the engineering team led by Artur Kubitzek and Udo Schminke at MPIDS, to Till Rehm, Markus Neumann and the staff at UFS for their technical help in building and installing our instruments at UFS. We are also thankful to Martin Hagen at the German Aerospace Center (DLR) and Reno Schafranek at DWD, who sent us the DWD data analyzed in this work. Financial support from the Max Planck Society, Leibniz Society, Deutsche Forschungsgemeinschaft (DFG) through the program SPP 1276 Metström, and the EU COST Action MP0806 "Particles in Turbulence" are gratefully acknowledged. We thank the Bayrisches Umweltminsterium for supporting the UFS as part of their mission.

The article processing charges for this open-access publication were covered by the Max Planck Society.

Edited by: M. Wendisch

References

Bodenschatz, E., Malinowski, S. P., Shaw, R. A., and Stratmann, F.: Can we understand clouds without turbulence?, Science, 327, 970–971, 2010.

Bourgoin, M., Ouellette, N. T., Xu, H., Berg, J., and Bodenschatz, E.: The role of pair dispersion in turbulent flow, Science, 311, 835–838, 2006.

Burattini, P., Lavoie, P., and Antonia, R. A.: On the normalized turbulent energy dissipation rate, Phys. Fluids, 17, 098103, doi:10.1063/1.2055529, 2005.

Devenish, B. J., Bartello, P., Brenguier, J.-L., Collins, L. R., Grabowski, W. W., IJzermans, R. H. A., Malinowski, S. P., Reeks, M. W., Vassilicos, J. C., Wang, L.-P., and Warhaft, Z.: Droplet growth in warm turbulent clouds, Q. J. Roy. Meteor. Soc., 138, 1401–1429, 2012.

DWD: Wetter und Klima – Deutscher Wetterdienst – Flächenpräsenz, available at: http://www.dwd.de/zugspitze (last access: 15 February 2015), 2000.

Engelbrecht, H.: Zugspitzplatt und Plattumrahmung, available at: http://www.umweltgeol-he.de/WerdenfelserGeotope.Wetterstein.ZugspitzplattUndPlattumrahmung.htm (last access: 13 January 2015), 2011.

Etling, D.: Theoretische Meteorologie: Eine Einführung, Springer, Berlin, Germany, 376 pp., 2008.

Frisch, U.: Turbulence: The legacy of A. N. Kolmogorov, Cambridge University Press, Cambridge, UK, 296 pp., 1995.

Jonas, P. R.: Turbulence and cloud microphysics, Atmos. Res., 40, 283–306, 1996.

Kolmogorov, A. N.: The local structure of turbulence in incompressible viscous fluid for very large Reynolds numbers, Dokl. Akad. Nauk SSSR, 30, 301–305, 1941.

La Porta, A., Voth, G. A., Crawford, A. M., Alexander, J., and Bodenschatz, E.: Fluid particle accelerations in fully developed turbulence, Nature, 409, 1017–1019, 2001.

Lumley, J. L. and Newman, G. R.: The Return to isotropy of homogeneous turbulence, J. Fluid Mech., 82, 161–178, 1977.

Mac Low, M.-M. and Klessen, R. S.: Control of start formation by supersonic turbulence, Rev. Mod. Phys., 76, 125–194, 2004.

Malinowski, S. P., Gerber, H., Jen-La Plante, I., Kopec, M. K., Kumala, W., Nurowska, K., Chuang, P. Y., Khelif, D., and Haman, K. E.: Physics of Stratocumulus Top (POST): turbulent mixing across capping inversion, Atmos. Chem. Phys., 13, 12171–12186, doi:10.5194/acp-13-12171-2013, 2013.

Monin, A. S. and Yaglom, A. M.: Statistical Fluid Mechanics, vol. 1, MIT Press, Cambridge, MA, 769 pp., 1971.

Monin, A. S. and Yaglom, A. M.: Statistical Fluid Mechanics, vol. 2, MIT Press, Cambridge, MA, 874 pp., 1975.

Mordant, N., Metz, P., Michel, O., and Pinton, J.-F.: Measurement of Lagrangian velocity in fully developed turbulence, Phys. Rev. Lett., 87, 214501, doi:10.1103/PhysRevLett.87.214501, 2001.

Mydlarski, L. and Warhaft, Z.: The onset of high-Reynolds-number grid-generated wind tunnel turbulence, J. Fluid Mech., 320, 331–368, 1996.

Pearson, B. R., Krogstad, P.-A., and van de Water, W.: Measurements of the turbulent energy dissipation rate, Phys. Fluids, 14, 1288–1290, 2002.

Pearson, B. R., Yousef, T. A., Haugen, N. E. L., Brandenburg, A., and Krogstad, P.-A.: Delayed correlation between turbulent energy injection and dissipation, Phys. Rev. E, 70, 056301, doi:10.1103/PhysRevE.70.056301, 2004.

Pope, S. B.: Turbulent flows, Cambridge University Press, Cambridge, UK, 2000.

Schumann, U.: Realizability of Reynolds-stress turbulence models, Phys. Fluids, 20, 721–725, 1977.

Shaw, R. A.: Particle-turbulence interactions in atmospheric clouds, Annu. Rev. Fluid Mech., 35, 183–227, 2003.

Siebert, H. and Teichmann, U.: Behaviour of an ultrasonic anemometer under cloudy conditions, Boundary Layer Meteor., 94, 165–169, 2000.

Siebert, H., Franke, H., Lehmann, K., Maser, R., Saw, E.-W., Schell, D., Shaw, R. A., and Wendisch, M.: Probing finescale dynamics and microphysics of clouds with helicopter-borne measurements, B. Am. Meteorol. Soc., 87, 1727–1738, 2006.

Siebert, H., Gerashchenko, S., Gylfason, A., Lehmann, K., Collins, L. R., Shaw, R. A., and Warhaft, Z.: Towards understanding the role of turbulence on droplets in clouds: In situ and laboratory measurements, Atmos. Res., 97, 426–437, 2010.

Siebert, H., Shaw, R. A., Ditas, J., Schmeissner, T., Malinowski, S. P., Bodenschatz, E., and Xu, H.: High-resolution measurement of cloud microphysics and turbulence at a mountaintop station, Atmos. Meas. Tech., 8, 3219–3228, doi:10.5194/amt-8-3219-2015, 2015.

Siebler, D.: Bestimmung von Größen- und Formfaktoren von Schnee anhand von Messungen am Schneefernerhaus, available at: http://elib.dlr.de/63396/ (last access: 13 January 2015), 2010.

Sreenivasan, K. R.: On the universality of the Kolmogorov constant, Phys. Fluids, 7, 2778–2784, 1995.

Sreenivasan, K. R.: An update on the energy dissipation rate in isotropic turbulence, Phys. Fluids, 10, 528–529, 1998.

Stull, R. B.: An Introduction to Boundary Layer Meteorology, Kluwer Academic Publishers, Dordrecht, the Netherlands, 670 pp., 1988.

Tennekes, T. and Lumley, J. L.: A First Course in Turbulence, The MIT Press, Cambridge, USA, 300 pp., 1972.

Wirth, V., Kristen, M., Leschner, M., Reuder, J., and Schween, J. H.: Banner clouds observed at Mount Zugspitze, Atmos. Chem. Phys., 12, 3611–3625, doi:10.5194/acp-12-3611-2012, 2012.

Wyngaard, J. C.: Turbulence in the Atmosphere, Cambridge University Press, New York, 406 pp., 2010.

Xu, H., Ouellette, N. T., Nobach, H., and Bodenschatz, E.: Experimental measurements of Lagrangian statistics in intense turbulence, in: Advances in Turbulence XI: Proc. 11th European Turbulence Conference, 25–28 June 2007, 1–10, 2009.

Zimmermann, R., Xu, H., Gasteuil, Y., Bourgoin, M., Volk, R., Pinton, J., and Bodenschatz, E.: The Lagrangian exploration module: An apparatus for the study of statistically homogeneous and isotropic turbulence, Rev. Sci. Instru., 81, 055112, doi:10.1063/1.3428738, 2010.